HHS Public Access

Author manuscript

Hum Genet. Author manuscript; available in PMC 2020 October 01.

Published in final edited form as:

Hum Genet. 2020 October ; 139(10): 1299–1314. doi:10.1007/s00439-020-02172-0.

Somatic mutations in planar cell polarity genes in neural tissue from human fetuses with neural tube defects

Tian Tian[1,2], **Yunping Lei**[3], **Yongyan Chen**[1,2], **Menuka Karki**[3], **Lei Jin**[1,2], **Richard H. Finnell**[3,4], **Linlin Wang**[1,2], **Aiguo Ren**[1,2]

[1]Ministry of Health Key Laboratory of Reproductive Health, Institute of Reproductive and Child Health, Peking University, Beijing 100191, China

[2]Department of Epidemiology and Biostatistics, School of Public Health, Peking University, Beijing, China

[3]Department of Molecular and Cellular Biology, Center for Precision Environmental Health, Baylor College of Medicine, Houston, TX, USA

[4]Departments of Molecular and Human Genetics and Medicine, Baylor College of Medicine, Houston, TX, USA

Abstract

Extensive studies that have sought causative mutation(s) for neural tube defects (NTDs) have yielded limited positive findings to date. One possible reason for this is that many studies have been confined to analyses of germline mutations and so may have missed other, non-germline mutations in NTD cases. We hypothesize that somatic mutations of planar polarity pathway (PCP) genes may play a role in the development of NTDs. Torrent™ Personal Genome Machine™ (PGM) sequencing was designed for selected PCP genes in paired DNA samples extracted from the tissues of lesion sites and umbilical cord from 48 cases. Sanger sequencing was used to validate the detected mutations. The source and distribution of the validated mutations in tissues from different germ layers were investigated. Subcellular location, western blotting, and luciferase

Linlin Wang linlinwang@bjmu.edu.cn, Aiguo Ren renag@bjmu.edu.cn.

Author contributions

LW, YL, and AR conceptualized the study; LW supervised the implementation and drafted the manuscript; TT conducted the functional study and drafted the manuscript; YL provided critical guidance on the functional study and interpretation of the results; YC helped with bench work; MK performed the cell migration assay; LJ participated in subject enrollment; and RHF critically revised the manuscript.

Tian Tian and Yunping Lei contributed equally to the manuscript.

Data availability

The datasets for this manuscript are not publicly available for ethical and legal reasons. Requests to access the datasets should be directed to LW at linlinwang@bjmu.edu.cn.

Conflict of interest

The authors declare that they have no conflict of interests.

Ethical approval

The study protocol was approved by the institutional review board of Peking University (Beijing, China, IRB00001052–18082).

Informed consent

Written informed consent was obtained from all of the mothers prior to the beginning of the investigation.

Electronic supplementary material

The online version of this article (https://doi.org/10.1007/s00439-020-02172-0) contains supplementary material, which is available to authorized users.

assays were performed to better understand the effects of the mutations on protein localization, protein level, and pathway signaling. ix somatic mutations were identified and validated, which showed diverse distributions in different tissues. Three somatic mutations were novel/rare: *CELSR1* p.Gln2125His, *FZD6* p.Gln88Glu, and *VANGL1* p.Arg374His. *FZD6* p.Gln88Glu caused mislocalization of its protein from the cytoplasm to the nucleus, and disrupted the colocalization of CELSR1 and FZD6. This mutation affected non-canonical WNT signaling in luciferase assays. *VANGL1* p.Arg374His impaired the co-localization of CELSR1 and VANGL1, increased the protein levels of VANGL1, and influenced cell migration. In all, 7/48 (14.5%) of the studied NTD cases contained somatic PCP mutations. Somatic mutations in PCP genes (e.g., *FZD6* and *VANGL1*) are associated with human NTDs, and they may occur in different stages and regions during embryonic development, resulting in a varied distribution in fetal tissues/organs.

Introduction

Neural tube defects (NTDs) are congenital malformations of the central nervous system that result from a failure of the neural tube to close during the third and fourth weeks post-fertilization (Wallingford et al. 2013). This term encompasses a number of distinct clinical entities, including anencephaly, spina bifida, craniorachischisis, encephalocele, iniencephaly, and others. Although NTDs are considered a multifactorial disorder, arising from complex interactions of genetic and environmental factors, the genetic components are the dominant factors contributing to failed neural tube closure (Copp and Greene 2010). Evidence from human studies shows a multifactorial polygenic or monogenic etiology of NTDs (Copp and Greene 2010; Greene et al. 2009). Association studies have identified common polymorphic variants, particularly in relation to folate one-carbon metabolism, as risk factors for NTDs (Copp and Greene 2010; Greene et al. 2009). Next-generation sequencing (NGS) studies in humans have revealed multiple genes, particularly for the planar cell polarity (PCP) signaling pathway, that may account for some NTD cases (Copp and Greene 2010; Greene et al. 2009).

The PCP signaling pathway plays an essential role in the polarization and coordinated movement of cells during embryonic morphogenesis (Juriloff and Harris 2012). Mutations in PCP genes could lead to NTD-related phenotypes in mice, and digenic, trigenic, and oligogenic combinations of PCP variants may also cause mouse NTDs (Harris and Juriloff 2010). There are several genes related to PCP that are pathogenic for human NTDs, including *VANGL2* (Lei et al. 2010), *VANGL1* (Kibar et al. 2007), *CELSR1* (Allache et al. 2012; Lei et al. 2014), *FZD* (De Marco et al. 2012), and *DVL* (De Marco et al. 2013).

At present, almost all reports of NTD-related mutations in humans are from studies that have used DNA extracted from blood or saliva samples, and the NTD-related mutations identified in these studies were all considered germline mutations. Germline mutations are zygotic variants that could lead to DNA changes in all cells of the fetus, while somatic mutations are postzygotic variants that can result in DNA variation between subsets of an organism’s cells in spite of undergoing development from a single fertilized egg (Poduri et al. 2013).

The importance of somatic mutations is well documented in cancer cells, and the contribution of somatic mutations to non-malignant disease has only been recognized

recently (Erickson 2010). Because mutations can occur randomly during mitotic cell division in embryonic development, somatic mutations are present in the clones of ensuing cells in one or more tissues of the body (Erickson 2010), including central nervous tissue. Given the exponential increase in cells during early neural development, a single mutation in a neural stem cell from the blastocyst can make a significant contribution to the embryo's neural tissue. Somatic mutations have been described in several neurodevelopmental disorders, including neurofibromatosis type 1 and 2 (Tinschert et al. 2000), early-onset Alzheimer's disease (Beck et al. 2004), hemimegalencephaly (Lee et al. 2012), and cerebral cortical malformations (Jamuar et al. 2014). Jamuar et al. (2014) reported a total of eight somatic mutations detected in cases with cerebral cortical malformations including double-cortex syndrome, periventricular nodular heterotopia, and pachygyria. Lee et al. (2012) identified de novo somatic mutations in the *PIK3CA*, *AKT3*, and *MTOR* genes from hemimegalencephaly cases. However, the role of somatic mutations in NTDs, a group of severe neurodevelopmental disorders, has not previously been explored.

Owing to the tremendous recent advances in DNA-sequencing technology, it is now possible to sensitively detect small levels of mosaicism in genomic DNA samples, which makes the detection of somatic mutations much easier and more sensitive than it had been previously. Thus, NGS can now be used to screen for somatic mutations. The analytical NGS platform can compare sequencing data for lesion tissue and matched normal tissue from the same individual to identify somatic mutations.

In the present study, we observed somatic mutations for the first time in PCP pathway genes from impaired neural tissues in NTD-affected fetuses, and we tested the source and distribution of the identified somatic mutations in multiple tissues, including skin, muscle, thymus, lung, and heart. We also performed functional studies on the somatic mutations identified to reveal the possible underlying biological mechanisms leading to failure of neural tube closure.

Materials and methods

Study population

The subjects were recruited from five rural counties of Shanxi Province (Xiyang, Shouyang, Taigu, Pingding, and Zezhou) in northern China from 2011 to 2014 (Wang et al. 2017). The NTD cases were fetuses terminated following the prenatal diagnosis of an NTD. Cephalic tissue from anencephalic cases and spinal cord tissue from cases with myelomeningocele were collected by experienced pathologists. For comparison, umbilical cord tissue (derived from the mesoderm), skin tissue (from the non-neural ectoderm), heart and muscle tissue (from the mesoderm), and thymus and lung tissue (from the entoderm) were also collected. Venous blood samples were collected from NTD case mothers at delivery or the time of termination of the NTD-affected pregnancies. Dried blood spots were collected from the fathers. Fetal tissue and maternal blood samples were stored at − 80 °C, and the dried blood spots were stored at − 20 °C until DNA extraction.

Paternity testing was performed on all of the available fetal and parental samples by genotyping a panel of polymorphic short tandem repeats to exclude false paternity and to establish that a parent was a study subject's actual biological parent.

The study protocol was approved by the institutional review board of Peking University (Beijing, China), and written informed consent was obtained from all of the mothers prior to the beginning of the investigation. Phenotypic information on the NTD cases is shown in Supplemental Table 1.

Pathological examination

Histopathological examination with HE staining was performed to confirm the type of tissue source for the genetic analyses (Fig. S1). The tissues were fixed in 10% neutral formalin overnight, stored in 70% ethanol, and embedded in paraffin. Sections of 4 μm were obtained, dewaxed, hydrated, and treated with 3% H_2O_2 to quench endogenous peroxidase. The paraffin sections were treated sequentially with xylene, ethanol at different concentrations (75%, 85%, and 95%; 2 min each), distilled water (2 min), Harris hematoxylin (1 min), 10% ethanol in acid (several seconds), flowing water (1 min), ethanol again at different concentrations (75%, 85%, and 95%; 2 min each), 1% eosin (1 min), 95% ethanol (several seconds), 100% ethanol (twice; 10 min each), and again with xylene (twice; 10 min each). The sections were mounted and observed under a light microscope, and representative photographs were captured.

DNA extraction

Fetal DNA from various tissue sources was extracted using the QIAamp DNA Mini Kit Tissue kit (Qiagen, Germany). Maternal DNA from blood was isolated using the QIAamp DNA Mini Kit Blood kit (Qiagen, Germany), and paternal DNA from dried blood spot was extracted using the QIAamp DNA Mini Kit Blood spot kit (Qiagen, Germany). The concentration of DNA was measured using the NanoDrop2000 Ultra-micro spectrophotometer (Thermo Fisher Scientific, USA). All of the DNA samples were stored at − 80 °C until analyzed.

Ion torrent personal genome machine (PGM) sequencing

To capture all exons and intron-exon boundaries for the target genes (RefSeq database, hg19 assembly), a multiplex amplification was designed online (Ion AmpliSeq Designer; https://www.ampliseq.com). The targeted gene panel included 14 genes: *CELSR1*, *DACT1*, *DVL1*, *DVL2*, *DVL3*, *FZD6*, *PRICKLE1*, *PRICKLE2*, *SCRIB*, *SEC24B*, *VANGL1*, *VANGL2*, *WNT5A*, and *GRHL3* (Supplemental Table 2). A total of 331 primer pairs were provided by the manufacturer (Life Technologies). The extracted DNA was electrophoresed to determine the degradation degree, then the genome DNA was diluted to 5 ng/μL. About 10 ng DNA was amplified by PCR using the premixed primer pool and the Ion AmpliSeq Library Kit 2.0. A water-in-oil reaction was performed with the Ion OneTouch™ 200 Solutions Kit v2 Instrument (Life Technologies). The enrichment of ion sphere particles (ISPs) was carried out on the Ion One-Touch ES instrument. The prepared samples were loaded onto a 318™ sequencing chip (Life Technologies), and the enriched ISPs were sequenced in the Ion PGM instrument. The raw data from the PGM runs were analyzed with the Coverage Analysis and

Variant Caller plugins available within the Torrent Suite™ Software from the PGM platform, and were annotated with Ion Reporter. The coverage data, identification of low-frequency mutations, and mutation annotation were achieved using the Ampliseq Tumor-Normal sample workflow within the Ion Reporter suite v4.6. The inclusion criteria for somatic mutation during this stage were (1) sequencing depth of mutation ≥ 100 × and alternate-allele read frequency in PGM > 5%; (2) $p \leq 5 \times 10^{-5}$; (3) frequency of mutation in broader population lower than 5%; and (4) missense or loss of function mutation.

PCR and Sanger sequencing validation

Sanger sequencing was used to validate the filtered protein-altering mutations in the target genes. The NCBI/Primer-BLAST online tool was used to design the PCR primers (Supplemental Table 3). The PCR reaction volume was 50 μL, composed of 2 × Taq PCR Green Mix 25 μL, ddH_2O 15 μL, forward and reverse primers 2 μL, and template DNA 6 μL (20 ng/μL). The PCR reaction program was as follows: 37 cycles of 94 °C for 12 min (94 °C for 30 s; 58 °C for 30 s; 72 °C for 30 s); 72 °C for 10 min; Sequencing was performed using the BigDye Terminator v3.1 Cycle Sequencing Kit and a 3130XL Genetic Analyzer (Applied Biosystems). The results were processed with Mutation Surveyor 4.0.8. The source and distribution were further explored for the validated mutants when DNA samples from tissues of skin, heart, muscle, thymus, and lung of the fetuses or the blood of the parents were available.

Plasmids

Mouse *Fzd6* cDNA was cloned into a Cherry-C1 plasmid (K4-*Fzd6*-Cherry) and pEGFP-C1 Mouse *Ceslr1* cDNA that was cloned into a pEGFP-N1 plasmid (pEGFPN1-*Celsr1*), obtained from Dr. Elaine Fuchs's laboratory (Devenport and Fuchs 2008) (The Rockefeller University, New York, USA). pcDNA3.1+/C-eGFP-*VANGL1* construct (clone ID: OHu10988) was purchased from the Genscript Company (Piscataway, NJ 08854, USA). *Fzd6* p.Gln88Glu and *VANGL1* p.Gly644Val mutations were introduced into their wild-type (WT) constructs through site-directed mutagenesis using GeneArt® Site-Directed Mutagenesis System (Thermo Fisher Scientific, CAT#: A14604). All plasmids were validated by sequencing analyses. M50 Super 8 × TOPFlash (Veeman et al. 2003a, b), human beta-catenin pcDNA3, and pcDNA3-S33Y beta-catenin (Kolligs et al. 1999) were purchased from Addgene (https://www.addgene.org/). The pAP1-Luc reporter construct (Part#: 219074) was purchased from Agilent.

Subcellular localization

MDCK II cells were purchased from Sigma-Aldrich and cultured in Eagle's minimum essential medium (Gibco™) supplemented with 10% heat-inactivated fetal bovine serum (FBS, Gibco™) and 1% Antibiotic-Antimycotic (Gibco™). Cultures were maintained at 37 °C in a humidified atmosphere containing 5% CO_2. Then, 20 h before transfection, cells were plated at a density of 3×10^5 cells per mL onto 18 mm coverslips (Corning, Corning, NY). Plasmids were transfected using Lipofectamine2000 (Invitrogen™), according to the manufacturer's protocol. After 48 h culturing, cells were fixed with 4% paraformaldehyde on coverslips for 15 min and then rinsed with PBS. Cells were blocked in 3% BSA for 1 h and then incubated in anti-rabbit-GFP (1:500, Abcam, MA, USA), anti-rabbit-VANGL1

(1:800, Cell Signaling Technology, Danvers, MA), and anti-rabbit-mCherry (1:2000, Abcam, MA, USA) overnight. After being rinsed three times with PBS, the cells were incubated with secondary antibody (1:2000; Alexa Fluor 647, Alexa Fluor 488, Life Technologies). Cells were finally stained with DAPI (300 ng/mL) for 2 min. Images were taken using a deconvolution microscope (Nikon T2).

Western blotting assay

HEK293T cells were grown in Dulbeco's modified Eagle's medium (Gibco™) supplemented with 10% heat-inactivated fetal bovine serum (FBS, Gibco™) and 1% Antibiotic-Antimycotic (Gibco™), and were maintained at 37 °C in a humidified atmosphere containing 5% CO_2. The cells were transfected with constructs of mCherry-*Fzd6* and GFP-*VANGL1* (WT or mutants) using Lipofectamine2000 and cultured for 48 h. Cells were rinsed with cold PBS twice and then lysed with 1 × NP40 Lysis buffer (Invitrogen™) with cOmplete™ ULTRA Tablets (Millipore Sigma) for 20 min. The protein lysates were immunoblotted with antirabbit-GFP, anti-mCherry, and anti-rabbit-GAPDH (1:1000, Cell Signaling, Danvers, MA, 2218S) overnight. IRDye® 800CW goat anti-rabbit IgG secondary antibodies (LI-COR, Cambridge, UK) were cultured for 1 h. The images were captured using Odyssey® (LI-COR). The statistical analyses were performed using a Student *t* test on data obtained from three independent experiments.

Live cell imaging for cell migration analyses

HEK293T cells were plated on 35 mm glass-bottomed microwell petri dishes (MatTek Corporation, Ashland, MA) at a confluence of 2.5×10^5. Then they were transfected with 1.5 μg GFP-*VANGL1* (WT or Mutant) or 1.5 μg mCherry-*FZD6* (WT or Mutant) using Lipofectamine 2000 and cultured for 24 h at 37 °C in an incubator supplied with 5% CO_2. Then the culture dish was placed into a temperature-controlled stage (Tokai Hit, Shizuoka-ken, Japan) pre-warmed at 37 °C and supplied with 5% CO_2. Images were acquired every 10 min for a total time of 2 h per condition using a CFI Plan Apochromat Lambda 20 ×, NA = 0.45, mounted on a Nikon Eclipse Ti2-E with Yokogawa W1 Spinning Disk Confocal Microscope and Photometrics Prime 95B sCMOS camera with NIS-Elements AR software. Then cell migration analyses were performed using a manual tracking method available in Fiji (ImageJ) software. Graphs were developed using Graphpad Prism software. All values are represented as the standard error of the mean (SEM). Statistical significance was determined using Student's *t* test, and *p* values of less than 0.05 were considered statistically significant.

Luciferase reporter assays

HEK293T cells were transfected with mCherry-*Fzd6* (WT or Mutant); GFP-*VANGL1* (WT or Mutant) along with TOP-Flash, which is a Wnt pathway signaling marker (Veeman et al. 2003a, b; Lei et al. 2015), or pAP1-Luc, which was used to measure activation of the non-canoncial Wnt/PCP pathway signaling (Lei et al. 2015); and Renilla-TK plasmid. Cells were lysed for 24 h post-transfection with passive lysis buffer (Promega, Madison, WI). The luciferase activity was measured using a Dual Luciferase Assay Kit (Promega, Madison, WI). The Biotek-2 plate reader was used to read the luminescence activity. A one-way ANOVA test was performed to compare the luciferase signaling among the three groups, and

then multiple comparisons between subgroups were performed using the multiple comparison method.

Bioinformatics and data analyses

The detected mutants were compared with the dbSNP (https://www.ncbi.nlm.nih.gov/snp), GenomAD, and ExAC (https://exac.broadinstitute.org/) databases. The effects of the mutations on protein function were predicted using SIFT (https://sift.jcvi.org/) and PolyPhen2 (https://genetics.bwh.harvard.edu/pph/). Clustal-Omega 1.2.1 software (https://www.ebi.ac.uk/Tools/msa/clustalo/) was used to estimate the conservation of proteins between different species. Localization of the mutations in their protein domains was assessed using Pfam 32.0 (https://pfam.xfam.org/). Mutation Surveyor 4.0.8 software was used to analyze Sanger sequencing data.

The relative protein level (mean ± SE) was analyzed using Student's *t* test, while the incidence of abnormal location cells between the WT and mutation groups was compared using a Chi-square test. Values of $p < 0.05$ were considered statistically significant.

Definition of somatic mutation

Umbilical cord tissue was designated as control tissue, as it is one of the earliest embryonic tissues to develop post-conception (Krzyzanowski et al. 2019). The mutation that occurred in the tissue at the site of the neural tube lesion but did not occur in the umbilical cord tissue of the same NTD case was defined as a somatic mutation (Knudson 1971).

Results

Somatic mutations identified by targeted next-generation sequencing

Paired tissue samples from neural tube lesions and umbilical cords from 48 NTD cases were collected and analyzed. A detailed pathological examination of the lesion tissue was performed. As shown in Figure S1, the cells of the spinal cord tissue from spina bifida fetuses showed more pyknosis, nuclear fragmentation, and karyolysis than those of the normal spinal cord tissue, indicating the degradation and necrosis of these cells. The cells of the brain tissue from anencephalic fetuses also showed more degradation than the control brain tissue.

Targeted NGS was performed on both lesion and umbilical cord DNA samples from the 48 NTD cases, after intronic and synonymous mutations were filtered and excluded, a total of 15 protein-altering somatic single nucleotide variants were located in 10 PCP genes, identified with a mean depth of approximately 480 × coverage (Table 1). Among the 15 somatic mutations, eight had alternate-allele read frequencies greater than 40%, and the alternate-allele read frequencies of seven were lower than 40%. Nine mutations were novel, not found in publicly available control databases, and five mutations were rare in control populations, with minor allele frequencies of less than 1%. Moreover, the mutations of *DACT1* c.1751T>A, *DVL1* c.1568G>T, *DVL3* c.1178G>A, *FZD6* c.1777C>A, *FZD6* c.1991C>A, *SCRIB* c.1931G>T, *VANGL1* c.1121G>A, *VANGL2* c.1088T>A, and c.1392C>G were predicted to be deleterious.

Validation by Sanger sequencing

To validate the identified mutations and further examine the source and distribution of the somatic mutations, Sanger sequencing was performed, using DNA isolated from tissues at the lesion site and from the epidermis, heart, muscles, thymus, and lungs of the NTD-affected fetuses and the blood of their parents. Mutations with alternate-allele read frequencies greater than 40% were validated (Table 2). Notably, all of the mutations showed diverse distributions in different tissues from different germ layers.

The mutations *CELSR1* c.6375G>C (A07), *DACT* c.1192C>T, *DVL2* c.1195A>G, *FZD6* c.1991A>C (A07, A18, A23), *FZD6* c.262C>G (A13), and *VANGL1* c.1121G>A (A13) only occurred in neural tube lesion tissues, indicating that these somatic mutations may only take place in the impaired neural tissues of NTD cases. *DVL2* c.1195A>G was detected in both lesions and skin tissue, both of which are from ectoderm, whereas neither were found in germ layers nor in the parents. *SCRIB* c.1931G>T and *CELSR1* c.1666C>G were identified not only in lesion tissue of fetus A05 but also in other tissues from all three germ layers, as well as in one of the parents, so they could have been inherited from one of the parents. We removed these two mutations from the somatic mutations and did not perform further functional analyses on them (Table 2).

Bioinformatics analyses for validated novel/rare somatic mutations

Among the six validated somatic mutations, *CELSR1* c.6375G>C (p.Gln2125His), *FZD6* c.262C>G (p.Gln88Glu), and *VANGL1* c.1121G>A (p.Arg374His) were novel mutations, suggesting that these three somatic variants may indicate risk for human NTDs. As shown in Fig. 1a, the *VANGL1* p.Arg374His mutant was located within the strabismus protein domain (Strabismus 2) of *VANGL1*. *FZD6* p.Gln88Glu was located in the Fz domain of FZD6, which is also known as the cysteine-rich domain. The *CELSR1* p.Gln2125Glu was not within the functional domain of the proteins. The conservation estimation showed that the amino acid position of *VANGL1* p.Arg374His is highly conserved in various species. *FZD6* p.Gln88Glu remains conserved within mammals. *CELSR1* p.Gln2125His is not conserved between species (Fig. 1b). Based on the bioinformatics data, we performed functional studies on *VANGL1* p.Arg374His and *FZD6* p.Gln88Glu. The Sanger sequencing chromatogram of these two mutations is shown in Fig. 2.

Effects of *FZD6* p.Gln88Glu and *VANGL1* p.Arg374His on protein levels and protein subcellular location

We initially examined the influence of identified mutations on protein subcellular location. The constructs of mCherry-*FZD6* (WT and mutant) and GFP-*VANGL1*(WT and mutant) were overexpressed in MDCKII cells. WT FZD6 was primarily located in the cytoplasm. However, FZD6 p.Gln88Glu was spread throughout not only the cytoplasm but also the nucleus (Fig. 3a). WT VANGL1 protein was expressed in the cytoplasm and plasma membrane. The VANGL1 p.Arg374His mutant proteins were observed throughout the cytoplasm, rather than being enriched in the plasma membrane. The fluorescence of the VANGL1 mutant protein was significantly higher than that of the WT, which implies that the mutation may affect the observed protein levels (Fig. 3c). Western blotting assays were performed, and although the *FZD6* mutation showed slightly higher protein levels than the

WT, there were no statistically significant differences between the two groups (Fig. 3b). However, the protein levels of VANGL1 p.Arg374His were significantly higher than the WT ($p < 0.05$), consistent with the immunofluorescence data in the subcellular assay, indicating that the mutations could enhance the expression or protein stability of *VANGL1* (Fig. 3d).

Co-localization of *FZD6* p.Gln88Glu and *VANGL1* p.Arg374His on the *CELSR-FZD6*/*CELSR-VANGL1* membrane

VANGL1 and FZD6 are membrane proteins that control cell polarity. They localize to cell contacts after combining with other proteins (Lei et al. 2015; Devenport et al. 2017). *Celsr1*, similar to Fmi in the *Drosophila* wing, is required to junctionally localize *Vangl1/2* and *Fzd6* (Devenport and Fuchs 2008; Strutt 2001; Bastock et al. 2003). Therefore, in this study, we co-transfected *Celsr1-Vangl1* (WT and mutant) and *Celsr1-FZD6* (WT and mutant) into MDCKII cells. As a result, WT FZD6 and the WT VANGL1 co-localized with Celsr1 at the point of cell-cell junction. *FZD6* p.Gln88Glu mutation caused Celsr1 and FZD6 to be expressed ubiquitously in cells, rather than being confined to the cell membrane. Similarly, *VANGL1* p.Arg374His and Celsr1 failed to co-locate to the cell membrane (Fig. 4a, c). The statistical analyses showed that, compared to WT groups, the incidences of abnormal localization in the VANGL1 p.Arg374His and FZD6 p.Gln88Glu groups were significantly higher (Fig. 4b, d).

The effect of *FZD6* p.Gln88Glu and *VANGL1* p.Arg374His on cell migration and canonical/non-canonical Wnt signaling pathway

The potential effects of the *FZD6* and *VANGL1* mutations on cell migration were examined by transfecting the constructs of *FZD6* (WT and mutant) and *VANGL1* (WT and mutant) into HEK293T cells (Fig. 5a). Neither the velocity nor the distance of cell migration between the *FZD6* WT and mutant group showed a significant difference (Fig. 5b, c). There were significant differences in the velocity and distance of cells transfected with *VANGL1* WT and mutant plasmids. The mutant of *VANGL1* showed higher velocity and longer distance than WT of *VANGL1* (Fig. 5d, e).

The topflash reporter gene was used to measure canonical WNT signaling in HEK293T cells, while the pAP1-Luc reporter gene was used to represent non-canonical expression levels in WNT signaling. Both the *FZD6* WT and mutant genes significantly downregulated canonical Wnt signaling. There were no differences between the WT and the mutant groups, indicating that p.Gln88Glu did not influence the regulation of FZD6 in terms of canonical Wnt signaling (Fig. 6a). WT *FZD6* did not show any significant differences from the negative control in AP1. However, the mutant showed significantly increased expression of AP1 ($p = 0.044$), which implies that *FZD6* p.Gln88Glu partially upregulated non-canonical Wnt signaling (Fig. 6b). As shown in Fig. 6c, both WT and mutated *VANGL1* negatively regulated the canonical Wnt signaling pathway ($p < 0.05$), but the two were not significantly different ($p = 0.829$). Moreover, WT *VANGL1* slightly decreased the non-canonical Wnt signaling pathway, while the mutation upregulated it. There was no significance between the neg-control and mutant group (Fig. 6d).

Discussion

All of the NTD-associated mutations reported in humans to date have been considered to be of possible germline origin. We detected somatic mutations in key PCP pathway genes in the neural tissues from NTD-affected fetuses for the first time. These may provide unique insight into the etiology of NTDs. Using targeted NGS in paired neural-umbilical cord DNA samples, we identified 15 NTD-related somatic mutations in 48 NTD-affected fetuses. Sanger sequencing is sensitive to somatic mutations at an alternate-allele read frequency greater than 17% (Jamuar et al. 2014), so we identified six variants with 17% or higher alternate-allele read frequencies on which to perform Sanger sequencing. Each was validated by Sanger sequencing. They varied in germ layer origin and in distribution among various organs and tissue samples. *CELSR1* p.Gln2125His, *FZD6* p.Gln88Glu, and *VANGL1* p.Arg374His are novel mutations. Functional studies demonstrated that *FZD6* p.Gln88Glu and *VANGL1* p.Arg374His affected the subcellular location of the protein, the protein level, and the effects of the genes on the canonical or non-canonical WNT pathway. These findings suggest that the somatic mutations of the PCP pathway genes in neural tissue could perhaps be associated with human NTDs.

Multiple animal studies and a few human studies related to germline mutations have clearly demonstrated that the PCP pathway genes play a critical role in neural tube closure. Frizzled (*FZD*s), Strabismus (STB), and Vang-like (*VANGLs*) are core genes in the PCP pathway and are essential to neural tube development (Schulte and Bryja 2007). Double-mutant $Fzd3^{-/-}/Fzd6^{-/-}$ embryos exhibited craniorachischisis and curled tail with a 100% penetrance (Wang et al. 2006), providing direct evidence for a functional connection between PCP components and the fusion processes of mammalian tissue, including neural tubes (Wang et al. 2006). Several human studies have reported germline mutations of FZD6 in different human NTD populations (De Marco et al. 2012; Shi et al. 2014). In the present study, we identified two somatic mutations (c.1991C>A [p.Ala664Glu] and c.262C>G [p.Gln88Glu]) in *FZD6* in NTD cases. FZD6 p.Gln88Glu is located in the Fz domain of FZD6, which is necessary and sufficient for Wnt ligand binding to the surface of expressing cells (Xu and Nusse 1998). A previous study reported that in the cells of the embryonic epidermal basal layer, Celsr1 is required to recruit Vangl2 and Fzd6 to sites for cell-cell contact, thus controlling cell polarity and driving the orientation of the hair follicles along the anterior-posterior axis (Devenport and Fuchs 2008). Cell functional assays showed that this mutation could lead to a mislocation of FZD6 from the cytoplasm to the nucleus, which would impair the co-localization of FZD6 and CELSR1 and partially upregulate non-canonical Wnt signaling. Thus, we assumed that the somatic mutant of *FZD6* c.262C>G may be associated with the occurrence of NTDs.

Vang1 is another key gene in the PCP pathway. It has four predicted transmembrane domains and a cytoplasmic domain that includes a PDZ-binding motif that mediates protein-protein interactions (Torban et al. 2004). Mice with *Vangl1* mutations display subtle changes in the polarity of the inner hair cells of the cochlea. Mice heterozygous for both *Vangl1* and *Vangl2* mutations present with severe craniorachischisis, inner ear defects, and cardiac abnormalities (Torban et al. 2008). Kibar et al. identified three mutations (p.Val238Ile, p.Arg274Gln, and p.Met328Thr) in the *VANGL1* gene in 144 Italian NTD patients (Kibar et

al. 2007). Bartsch et al. performed direct sequencing of the *VANGL1* gene and identified three different heterozygous missense mutations (p.Arg173His, p.Arg186His, and p.Gly205Arg) in 3 of 144 unrelated patients with various forms of NTDs from Slovakia, Romania, and Germany (Bartsch et al. 2012). However, these findings are mainly about germline mutations. Our study detected a novel somatic mutation of *VANGL1* c.1121G>A p.Arg374His, which was validated by Sanger sequencing. The *VANGL1* p.Arg374His mutant was located within the strabismus protein domain (Strabismus 2) of *VANGL1*, which is implicated in the binding of several other PCP genes (Katoh and Katoh 2005; Katoh 2002). We further examined functional changes in this variant. We determined that the p.Arg374His *VANGL1* mutation increased the protein level of VANGL1 and disturbed the co-dependent localization of this VANGL1 with CELSR in relation to the cell membrane and influenced the migration of cells, which implies that the somatic mutation of *VANGL1* is likely pathogenic for NTDs.

In all vertebrates, the gastrulating embryo forms a gastrula with either two or three layers during early embryogenesis. The three layers found in human embryos, called germ layers, differentiate into all adult tissues and organs. Henrique et al. (2015) showed that after gastrulation, the ectoderm and mesoderm (perhaps also the endoderm) can arise from single neuro-mesodermal progenitor (NMP) cells in the caudal region of the embryo and the whole lower spinal cord is formed from NMPs (Henrique et al. 2015). In this study, the somatic mutations were identified from the neural tissues of NTD-affected fetuses, which developed from the neural ectoderm or NMPs. We further examined the source and distribution of these somatic mutations in different tissues from three germ layers, including the epidermis, derived from the ectoderm; the heart and muscle tissues, which are mesoderm in origin; and the thymus and lungs, which are from the endoderm. Their distribution suggested that these somatic mutations might occur at different developmental stages and within different regions during the course of embryogenesis. In NTD parents whose offspring were identified as having somatic mutations, the corresponding mutations were also detected in blood samples of those that were available for study. We found that somatic mutations of *DVL2* c.1195A>G, *FZD6* c.262C>G, and *VANGL1* c.1121G>A were absent in parents and in other normal organs, indicating that these mutations were not inherited from their parents and occurred in the neural tissue of the fetus. In addition, some mutations, considered in reference to somatic changes in the fetus, were detected in other normal organs from different germ layers, which implies that gene somatic mutations may happen randomly anytime and anywhere during embryonic development.

This study represents the first examination of somatic mutations in NTDs. The genetic information in DNA can be changed through either inducibility or spontaneity at any time when the cell is at rest or actively engaged in transcription, replication, or repair. A mutation may arise when an incomplete repair or misrepair occurs, although most lesions in DNA are repaired by cellular repair mechanisms. There is a significant body of evidence demonstrating that initiation of cancer is driven by clones carrying somatic mutations (Erickson 2010; Sorsa 1980). Similarly, embryonic development is characterized by rapid proliferation and differentiation. An early-stage mutation in an embryonic stem cell in the blastocyst can affect all of the cells within the organism that are differentiated from the mutation-carrying clone. The central nervous system seems particularly vulnerable to

somatic mosaicism, given its exponential division rate, which might explain the potential role of somatic mutations in the etiology of congenital malformations of the central nervous system, including NTDs.

At present, there is no consistent conclusion about the relationship between somatic mutation and neurodegeneration. Several previous studies have reported that somatic mutations may affect cell proliferation and survival and contribute to neurodegeneration (Leija-Salazar et al. 2018; McConnell et al. 2017). Those findings on some level support our hypothesis that somatic mutation may be the cause of neurodegeneration. On the other hand, other studies have found that harmful items during neurodegeneration would cause DNA breaks that are genome wide (Suberbielle et al. 2013; Violet et al. 2015). Because neural tissues can only be obtained after the closure failure of the neural tube is confirmed and at the time of pregnancy termination, tissue degeneration is inevitable. Therefore, we cannot completely rule out the possibility that the somatic mutations identified in this study were caused by tissue degeneration. However, the fact that the two identified mutations of *FZD6* and *VANGL1* had a series of influences on protein functions supports our hypothesis that the mutations are causes rather than consequences of neural tube closure failure. Obviously, further studies are needed to confirm our findings.

Previous chimera studies of the loop-tail (Vangl2) mouse mutant combined both mutant and WT cells in all tissues of the embryo and showed that the proportion of mutated cells determines the phenotype of NTDs (Musci and Mullen 2003; Ybot-Gonzalez et al. 2007). Those with high proportions of mutant cells develop NTDs, and those with low proportions develop normally, implying that the somatic mutation of PCP pathway genes may play a potentially important role in the occurrence of NTDs. In the PGM sequencing of this study, alternate-allele read frequencies could reflect the percentage of mutant reads to total reads. Six mutations with more than 40% altered allele frequencies in neural tissues were validated, with a mutation burden of 42.0–55.9% in neural tissues. The detected somatic mutation sites did not show in the umbilical cord tissue. As the human genome is diploid and these mutations are supposed to be present in only one of two alleles, we infer that a substantially higher percentage (perhaps more than 80%) of cells carry mutations in these lesion regions. This frequency is high enough to cause disorders during neural tube closure.

In conclusion, we found that somatic mutations of core PCP pathway genes in neural tissues may be related to the formation of NTDs. These somatic mutations could occur at different stages and in different regions during embryonic development, resulting in varied distributions in the fetal tissues/organs. Further study is required to examine the tissue specificity or mechanisms of somatic mutations leading to mosaicism.

Supplementary Material

Refer to Web version on PubMed Central for supplementary material.

Funding

This work was supported by the National Natural Science Foundation of China (Grant No. 81773441). Dr. Richard Finnell was supported in part by funds made available from the William T. Butler, M.D., Distinguished Chair endowment at Baylor College of Medicine and a grant from the National Institutes of Health (HD081216).

References

Allache R, De Marco P, Merello E, Capra V, Kibar Z (2012) Role of the planar cell polarity gene CELSR1 in neural tube defects and caudal a genesis. Birth Defects Res A Clin Mol Teratol 94:176–181. 10.1002/bdra.23002 [PubMed: 22371354]

Bartsch O, Kirmes I, Thiede A, Lechno S, Gocan H, Florian IS, Haaf T, Zechner U, Sabova L, Horn F (2012) Novel VANGL1 gene mutations in 144 Slovakian, Romanian and German patients with neural tube defects. Mol Syndromol 3:76–81. 10.1159/000339668 [PubMed: 23326252]

Bastock R, Strutt H, Strutt D (2003) Strabismus is asymmetrically localised and binds to Prickle and Dishevelled during *Drosophila* planar polarity patterning. Development 130:3007–3014. 10.1242/dev.00526 [PubMed: 12756182]

Beck JA, Poulter M, Campbell TA, Uphill JB, Adamson G, Geddes JF, Revesz T, Davis MB, Wood NW, Collinge J (2004) Somatic and germline mosaicism in sporadic early-onset Alzheimer's disease. Hum Mol Genet 13:1219–1224. 10.1093/hmg/ddh134 [PubMed: 15115757]

Copp AJ, Greene ND (2010) Genetics and development of neural tube defects. J Pathol 220:217–230. 10.1002/path.2643 [PubMed: 19918803]

De Marco P, Merello E, Rossi A, Piatelli G, Cama A, Kibar Z, Capra V (2012) FZD6 is a novel gene for human neural tube defects. Hum Mutat 33:384–390. 10.1002/humu.21643 [PubMed: 22045688]

De Marco P, Merello E, Consales A, Piatelli G, Cama A, Kibar Z, Capra V (2013) Genetic analysis of disheveled 2 and disheveled 3 in human neural tube defects. J Mol Neurosci 49:582–588. 10.1007/s12031-012-9871-9 [PubMed: 22892949]

Devenport D, Fuchs E (2008) Planar polarization in embryonic epidermis orchestrates global asymmetric morphogenesis of hair follicles. Nat Cell Biol 10:1257–1268. 10.1038/ncb1784 [PubMed: 18849982]

Devenport D, Oristian D, Heller E, Fuchs E (2017) Corrigendum: mitotic internalization of planar cell polarity proteins preserves tissue polarity. Nat Cell Biol 19:143 10.1038/ncb3469 [PubMed: 28139653]

Erickson RP (2010) Somatic gene mutation and human disease other than cancer: an update. Mutat Res 705:96–106. 10.1016/j.mrrev.2010.04.002 [PubMed: 20399892]

Greene ND, Stanier P, Copp AJ (2009) Genetics of human neural tube defects. Hum Mol Genet 18:R113–129. 10.1093/hmg/ddp347 [PubMed: 19808787]

Harris MJ, Juriloff DM (2010) An update to the list of mouse mutants with neural tube closure defects and advances toward a complete genetic perspective of neural tube closure. Birth Defects Res A Clin Mol Teratol 88:653–669. 10.1002/bdra.20676 [PubMed: 20740593]

Henrique D, Abranches E, Verrier L, Storey KG (2015) Neuromesodermal progenitors and the making of the spinal cord. Development 17:2864–2875. 10.1242/dev.119768

Jamuar SS, Lam AT, Kircher M, D'Gama AM, Wang J, Barry BJ, Zhang X, Hill RS, Partlow JN, Rozzo A et al. (2014) Somatic mutations in cerebral cortical malformations. N Engl J Med 371:733–743. 10.1056/NEJMc1411784 [PubMed: 25140959]

Juriloff DM, Harris MJ (2012) A consideration of the evidence that genetic defects in planar cell polarity contribute to the etiology of human neural tube defects. Birth Defects Res A Clin Mol Teratol 94:824–840. 10.1002/bdra.23079 [PubMed: 23024041]

Katoh M (2002) Molecular cloning and characterization of Strabismus 2 (STB2). Int J Oncol 20:993–998. 10.3892/ijo.20.5.993 [PubMed: 11956595]

Katoh Y, Katoh M (2005) Comparative genomics on Vangl1 and Vangl2 genes. Int J Oncol 26:1435–1440. 10.3892/ijo.26.5.1435 [PubMed: 15809738]

Kibar Z, Torban E, McDearmid JR, Reynolds A, Berghout J, Mathieu M, Kirillova I, De Marco P, Merello E, Hayes JM (2007) Mutations in VANGL1 associated with neural-tube defects. N Engl J Med 356:1432–1437. 10.1056/NEJMoa060651 [PubMed: 17409324]

Knudson AG Jr (1971) Mutation and cancer: statistical study of retinoblastoma. Proc Natl Acad Sci USA 68:820–823. 10.1073/pnas.68.4.820 [PubMed: 5279523]

Kolligs FT, Hu G, Dang CV, Fearon ER (1999) Neoplastic transformation of RK3E by mutant beta-catenin requires deregulation of Tcf/Lef transcription but not activation of c-myc expression. Mol Cell Biol 19:5696–5706. 10.1128/mcb.19.8.5696 [PubMed: 10409758]

Krzyzanowski A, Kwiatek M, Geca T, Stupak A, Kwasniewska A (2019) Modern ultrasonography of the umbilical cord: prenatal diagnosis of umbilical cord abnormalities and assessement of fetal wellbeing. Med Sci Monit 25:3170–3180. 10.12659/MSM.913762 [PubMed: 31036798]

Lee JH, Huynh M, Silhavy JL, Kim S, Dixon-Salazar T, Heiberg A, Scott E, Bafna V, Hill KJ, Collazo A et al. (2012) De novo somatic mutations in components of the PI3K-AKT3-mTOR pathway cause hemimegalencephaly. Nat Genet 44:941–945. 10.1038/ng.2329 [PubMed: 22729223]

Lei YP, Zhang T, Li H, Wu BL, Jin L, Wang HY (2010) VANGL2 mutations in human cranial neural-tube defects. N Engl J Med 362:2232–2235. 10.1056/NEJMc0910820 [PubMed: 20558380]

Lei YP, Zhu H, Yang W, Ross ME, Shaw GM, Finnell RH (2014) Identification of novel CELSR1 mutations in spina bifida. PLoS ONE 9:e92207 10.1371/journal.pone.0092207 [PubMed: 24632739]

Lei YP, Fathe K, McCartney D, Zhu H, Yang W, Ross ME, Shaw GM, Finnell RH (2015) Rare LRP6 variants identified in spina bifida patients. Hum Mutat 36:342–349. 10.1002/humu.22750 [PubMed: 25546815]

Leija-Salazar M, Piette C, Proukakis C (2018) Review: somatic mutations in neurodegeneration. Neuropathol Appl Neurobiol 44:267–285. 10.1111/nan.12465 [PubMed: 29369391]

McConnell MJ, Moran JV, Abyzov A, Akbarian S, Bae T, Cortes-Ciriano I et al. (2017) Intersection of diverse neuronal genomes and neuropsychiatric disease: the brain somatic mosaicism network. Science 356:6336 10.1126/science.aal1641

Musci TS, Mullen RJ (2003) All-or-none craniorachischisis in loop-tail mutant mouse chimeras. Development 110:229–237

Poduri A, Evrony GD, Cai X, Walsh CA (2013) Somatic mutation, genomic variation, and neurological disease. Science 341:1237758 10.1126/science.1237758 [PubMed: 23828942]

Schulte G, Bryja V (2007) The Frizzled family of unconventional G-protein-coupled receptors. Trends Pharmacol Sci 28:518–525. 10.1002/humu.21662 [PubMed: 17884187]

Shi OY, Yang HY, Shen YM, Sun W, Cai CY, Cai CQ (2014) Polymorphisms in FZD3 and FZD6 genes and risk of neural tube defects in a northern Han Chinese population. Neurol Sci 35:1701–1706. 10.1007/s10072-014-1815-4 [PubMed: 24816679]

Sorsa M (1980) Somatic mutation theory. J Toxicol Environ Health 6:977–982. 10.1080/15287398009529919 [PubMed: 7463528]

Strutt DI (2001) Asymmetric localization of Frizzled and the establishment of cell polarity in the *Drosophila* wing. Mol Cell 7:367–375. 10.1016/s1097-2765(01)00184-8 [PubMed: 11239465]

Suberbielle E, Sanchez PE, Kravitz AV, Wang X, Ho K, Eilertson K, Devidze N, Kreitzer AC, Mucke L (2013) Physiologic brain activity causes DNA double-strand breaks in neurons, with exacerbation by amyloid-beta. Nat Neurosci 16:613–621. 10.1038/nn.3356 [PubMed: 23525040]

Tinschert S, Naumann I, Stegmann E, Buske A, Kaufmann D, Thiel G, Jenne DE (2000) Segmental neurofibromatosis is caused by somatic mutation of the neurofibromatosis type 1 (NF1) gene. Eur J Hum Genet 8:455–459. 10.1038/sj.ejhg.5200493 [PubMed: 10878667]

Torban E, Wang HJ, Groulx N, Gros P (2004) Independent mutations in mouse Vangl2 that cause neural tube defects in looptail mice impair interaction with members of the Dishevelled family. J Biol Chem 279:52703–52713. 10.1074/jbc.M408675200 [PubMed: 15456783]

Torban E, Patenaude AM, Leclerc S, Rakowiecki S, Gauthier S, Andelfinger G, Epstein DJ, Gros P (2008) Genetic interaction between members of the Vangl family causes neural tube defects in mice. Proc Natl Acad Sci USA 105:3449–3454. 10.1073/pnas.0712126105 [PubMed: 18296642]

Veeman MT, Axelrod JD, Moon RT (2003a) A second canon. Functions and mechanisms of beta-catenin-independent Wnt signaling. Dev Cell 5:367–377. 10.1016/s1534-5807(03)00266-1 [PubMed: 12967557]

Veeman MT, Slusarski DC, Kaykas A, Louie SH, Moon RT (2003b) Zebrafish prickle, a modulator of noncanonical Wnt/Fz signaling, regulates gastrulation movements. Curr Biol 13:680–685. 10.1016/s0960-9822(03)00240-9 [PubMed: 12699626]

Violet M, Chauderlier A, Delattre L, Tardivel M, Chouala MS, Sultan A, Marciniak E, Humez S et al. (2015) Prefibrillar Tau oligomers alter the nucleic acid protective function of Tau in hippocampal neurons in vivo. Neurobiol Dis 82:540–551. 10.1016/j.nbd.2015.09.003 [PubMed: 26385829]

Wallingford JB, Niswander LA, Shaw GM, Finnell RH (2013) The continuing challenge of understanding, preventing, and treating neural tube defects. Science 339:1222002 10.1126/science.1222002 [PubMed: 23449594]

Wang Y, Guo N, Nathans J (2006) The role of Frizzled3 and Frizzled6 in neural tube closure and in the planar polarity of inner-ear sensory hair cells. J Neurosci 26:2147–2156. 10.1523/JNEUROSCI.4698-05.2005 [PubMed: 16495441]

Wang L, Lin S, Yi D, Huang Y, Wang C, Jin L, Liu J, Zhang Y, Ren A (2017) Apoptosis, expression of PAX3 and P53, and caspase signal in fetuses with neural tube defects. Birth Defects Res 109:1596–1604. 10.1002/bdr2.1094 [PubMed: 28786179]

Xu YK, Nusse R (1998) The Frizzled CRD domain is conserved in diverse proteins including several receptor tyrosine kinases. Curr Biol 8:R405–406. 10.1016/s0960-9822(98)70262-3 [PubMed: 9637908]

Ybot-Gonzalez P, Savery D, Gerrelli D, Signore M, Mitchell CE, Faux CH, Greene ND, Copp AJ (2007) Convergent extension, planar-cell-polarity signalling and initiation of mouse neural tube closure. Development 134:789–799. 10.1242/dev.000380 [PubMed: 17229766]

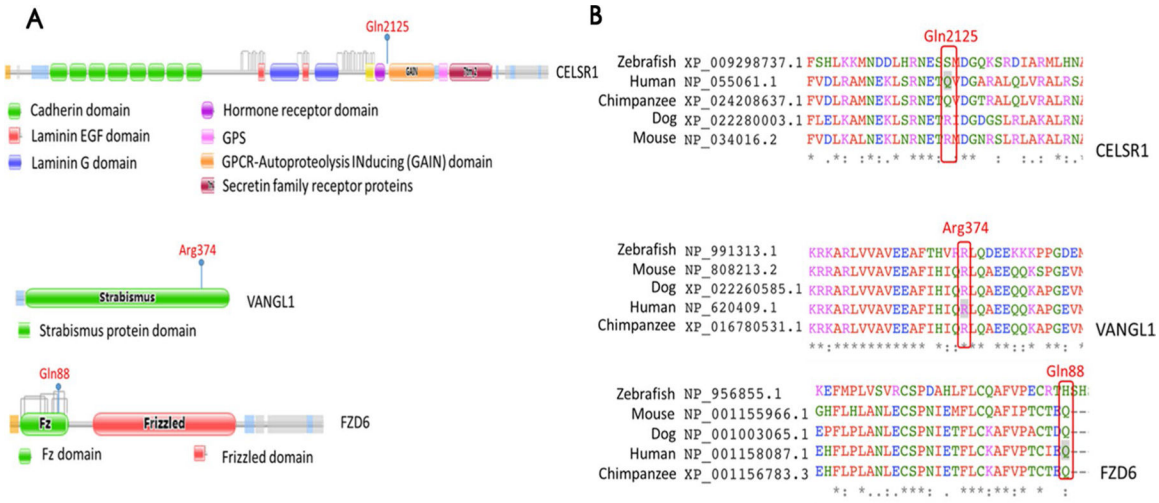

Fig. 1.

Bioinformatic analyses of the four validated somatic mutations. **a** Conserved domains, total scheme of target genes, and positions of the detected mutations. **b** Partial alignment of human target PCP pathway genes with four other orthologous sequences

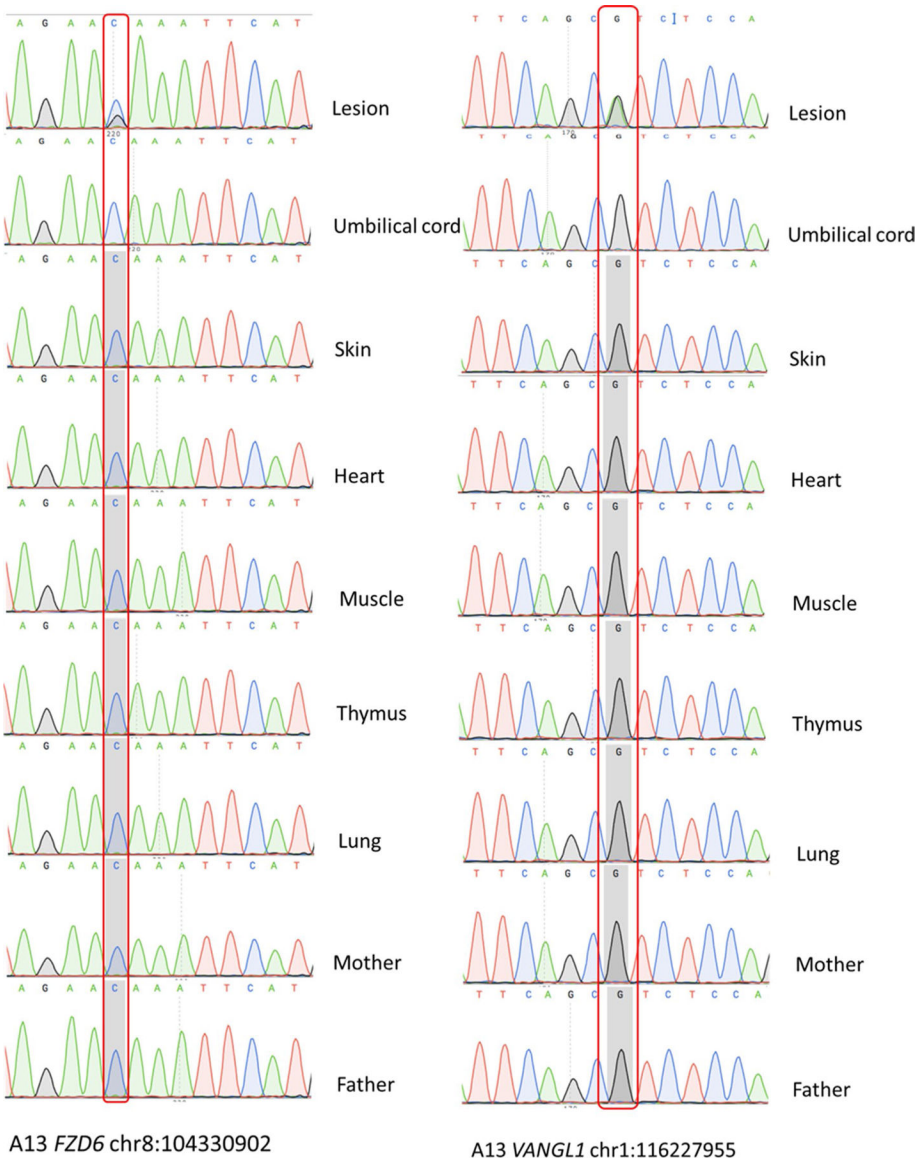

Fig. 2.

Sanger sequencing map of *VANGL1* and *FZD6* in sample A13. A heterozygous mutation of *FZD6* c.262C>G is shown in a lesion from NTD case A13. No evidence for the c.262C>G mutation was found in DNA obtained from umbilical cords, skin, hearts, muscles, thymus, or lungs from NTD cases or from the blood of their parents. Similarly, a heterozygous mutation of *VANGL1* c.1121G>A was found in the NTD lesion site but not in other normally formed organs nor in the blood of the parents. The color codes for the nucleotide peaks are A, green; T, red; C, blue; and G, black. The positions of interest are highlighted by vertical red lines

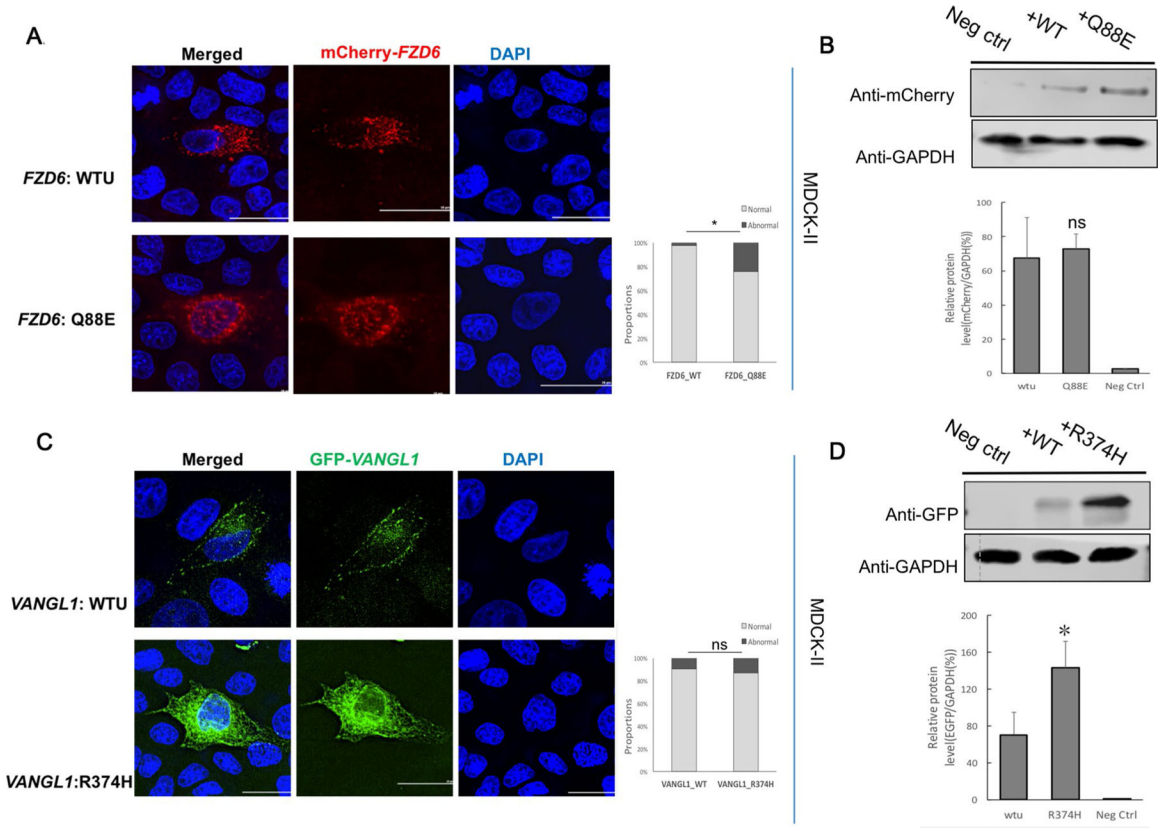

Fig. 3.

Mutated constructs affect subcellular localization of FZD6 and VANGL1 and their protein level. **a** MDCK-II cells were transfected with mutant and wild-type constructs of mCherry-*FZD6* for 48 h incubation and then were imaged under a deconvolution microscope. *WT/WTU* wild type. **b** HEK293T cells were transfected with mCherry-*FZD6* (WT and mutants) for 48 h and then Western blotting assays were performed to determine the protein levels. The predicted size of WT and mutant constructs were 108 KD. A Western blotting assay was repeated three times, and *t* tests of the relative expression for GAPDH were compared between the WT and the mutant group; *ns* not significant. **c** MDCK-II cells were transfected with mutated and wild-type constructs of GFP-*VANGL1* for 48 h incubation and were imaged under a deconvolution microscope. *WT* wild type. **d** HEK293T cells were transfected with GFP-*VANGL1* (WT and mutants) and a Western blotting assay was performed. The predicted sizes of WT and the mutant constructs are 85 KD. A Western blotting assay was repeated three times and *t* tests of the relative expression for GAPDH were compared between WT and the mutated group. *$p < 0.05$

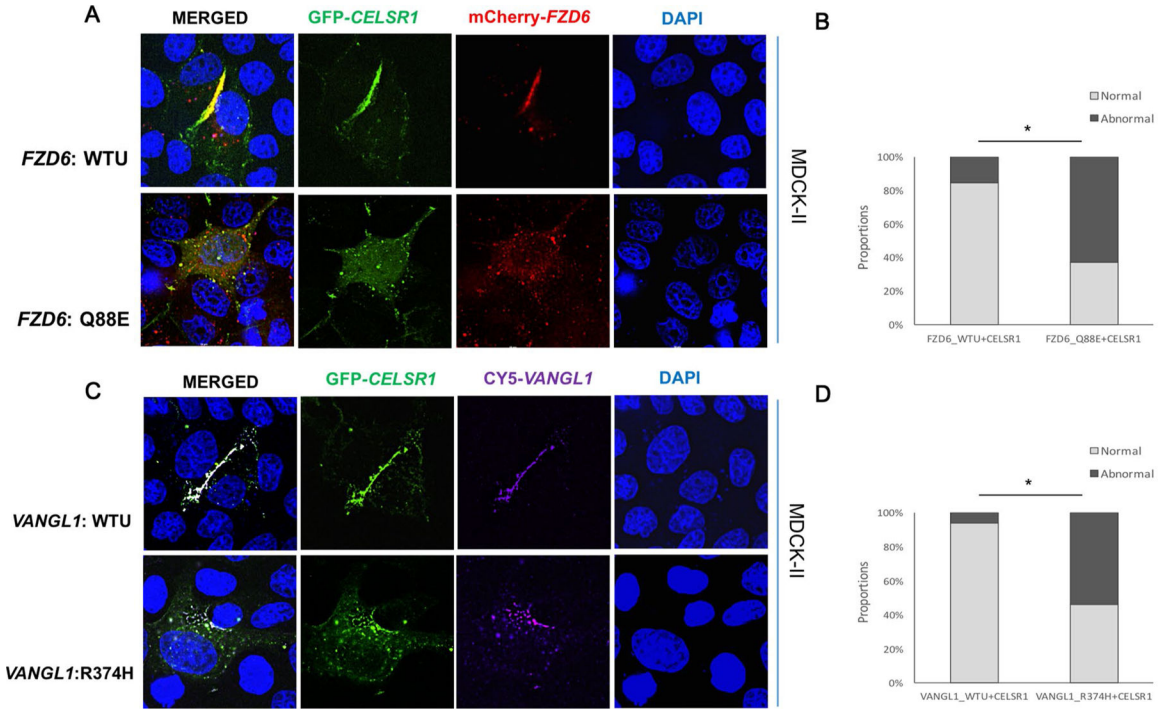

Fig. 4.

Co-localization of FZD6 with CELSR1, VANGL1 with CELSR1. **a** The MDCK-II cells were co-transfected with GFP-*Celsr1* (green) and mCherry-*FZD6* (red). Then an immunostaining assay was performed to examine the subcellular co-localization of the wild-type (WT) and mutated group with CLESR1. The WT of the *FZD6* construct was co-localized with Celsr1 to cell-cell borders, while the mutant of *FZD6* affected the transfer of FZD6 and Celsr1 to the cell border. **b** Under the microscope, ten field versions were selected randomly, and the proportion of the mislocated cells was calculated. The proportions of mislocated cells in the WT group and mutated group were compared using a Chi-square test. Normal: FZD6 and Celsr1 were co-localized to the cell and the cell border. Abnormal: FZD6 or Celsr1 failed to localize to the cell-cell contact. **c** The MDCK-II cells were co-transfected with GFP-*Celsr1* (green) and GFP-*VANGL1* (CY5). An immunostaining assay was performed to examine the sub-cellular co-localization of the WT and mutated group with CLESR1. The cells were stained with anti-*VANGL1* primary antibody and Alexa Fluor 647 secondary antibody. The signal of VANGL1 was observed on the CY5 channel. The WT of VANGL1 was co-localized with Celsr1 to cell-cell borders, while the mutant of *VANGL1* failed to transfer *Celsr1* to the cell border. **d** Under the microscope, ten field versions were selected randomly and the proportion of the mislocated cells were calculated. The proportions of mislocated cells in the WT group and in the mutated group were compared using a chi-square test. Normal: the VANGL1 and Celsr1 were co-localized to the cell and cell border. Abnormal: VANGL1 or Celsr1 failed to localize to the cell-cell contact

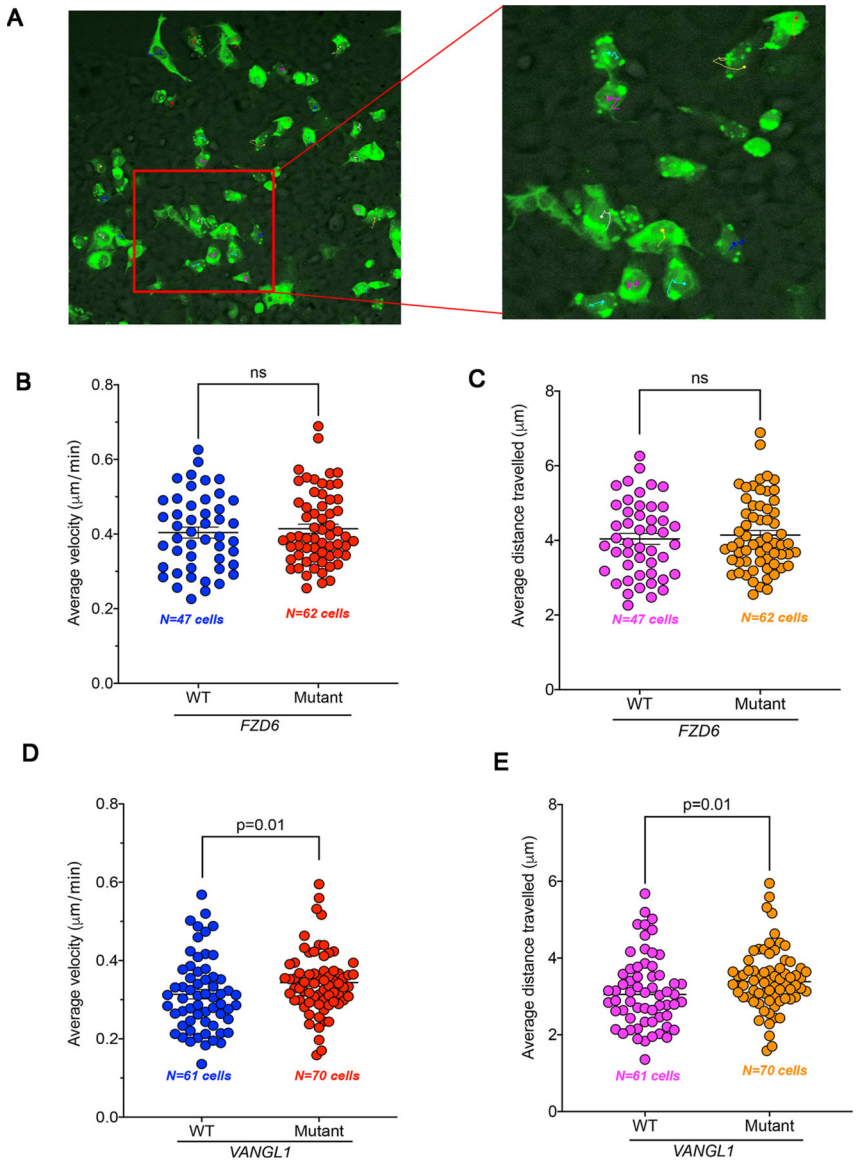

Fig. 5.

Single-cell tracking and collective migration analyses. **a** Representation of the trajectory of HEK293T cells (here transfected with mutant GFP-*VANGL1*) to determine migration velocity and distance traveled. **b** Graph showing the comparison of the average migration velocity of cells transfected with *FZD6* wild-type (WT) and mutant constructs. **c** Graph comparing the average migrating distance of the cells transfected with *FZD6* WT and mutant constructs. **d** Graph representing the average migration velocity of the cells transfected with *VANGL1* WT and mutant constructs. **e** Average migration distance of cells transfected with *VANGL1* WT and mutant constructs. The statistically significant differences were determined using Student's *t* test. Values of *p* less than 0.05 were considered statistically significant; ns, nonsignificant

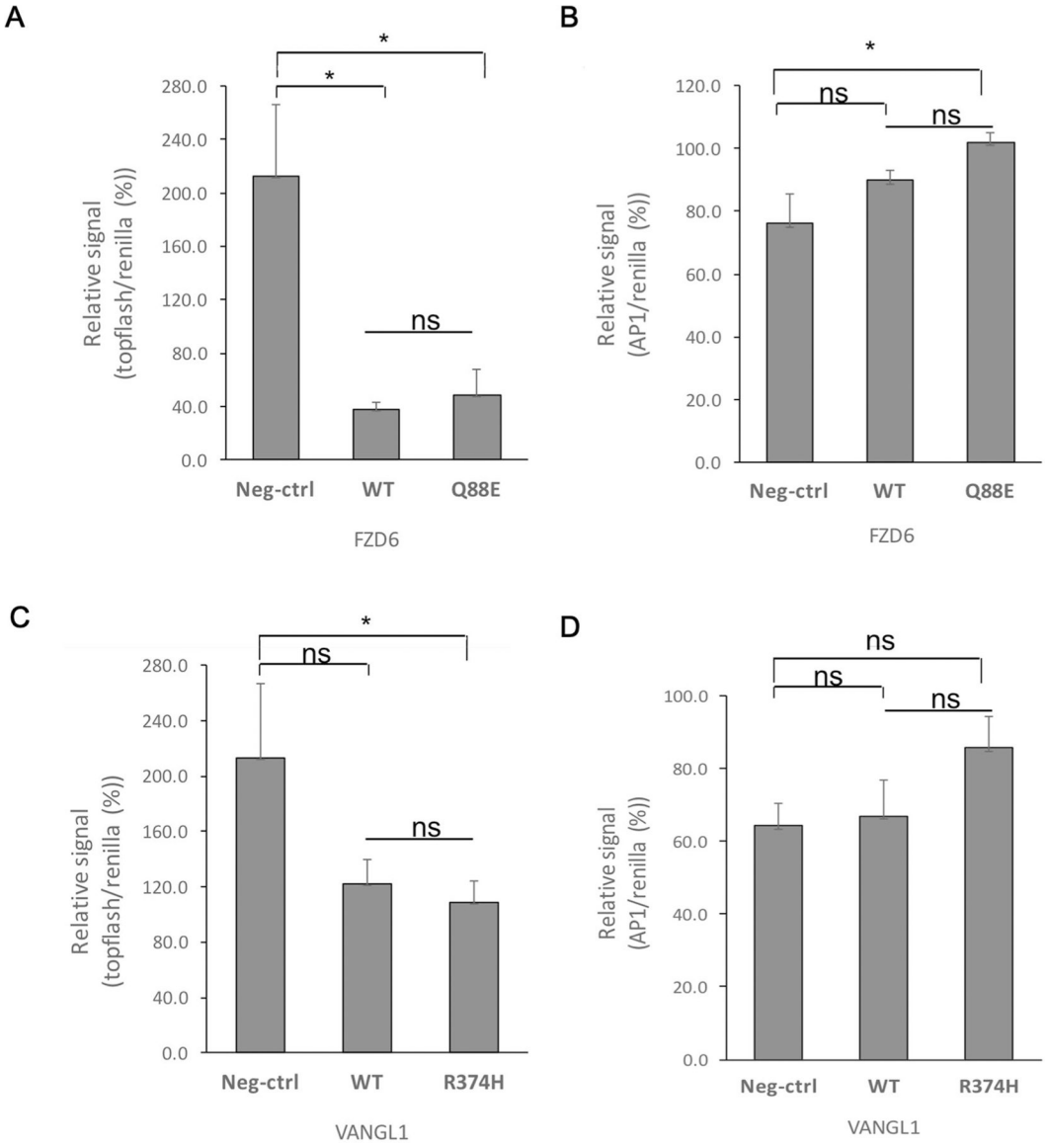

Fig. 6.

Luciferase assay for non-canonical/canonical Wnt signaling pathway. A one-way ANOVA test was performed first to compare luciferase signaling among the three groups, and multiple comparisons was subsequently carried out between subgroups using the LSD method. Topflash signal relative to Renilla represents canonical WNT signaling, in which the AP1 represents non-canonical WNT signaling. **a** The effects of *FZD6* on canonical WNT signaling. An ANOVA test showed that there were significant differences among the three groups ($p = 0.016$). Both WT and mutant *FZD6* decreased canonical WNT signaling, but there was no difference between WT and mutant. **b** The effects of *FZD6* on non-canonical WNT signaling. There were no significant differences among the three groups (ANOVA test, $p = 0.055$). However, multiple comparisons showed that compared to negative control, the *FZD6* mutation increased non-canonical WNT signaling pathway expression ($p = 0.020$). **c** The effects of *VANGL1* on canonical WNT signaling. The three groups did not show any

significant differences (ANOVA test, $p = 0.099$). The mutant *VANGL1* showed decreased canonical WNT signaling compared to negative control ($p = 0.049$). **d** The effects of *VANGL1* on non-canonical WNT signaling. An ANOVA test and multiple comparison tests showed that *VANGL1* WT and mutant did not influence the non-canonical WNT signaling pathway. *Significant ($p < 0.05$) regulation; *ns* nonsignificant

Table 1

Somatic mutations identified in 48 NTD cases

Gene	Sample ID	Locus (37)	Coding	Amino acid change	Transcript	Variant effect	Altered allele-freq. (%)	Cov	Freq. in Genomad	dbSNP	SIFT	PolyPhen
CELSR1	A05	chr22:46931402	c.1666C>G	p.Leu556Val	NM_014246.1	Missense	47.7	690	0.015	rs11575871	0.84	0.092
	A07	chr22:46785367	c.6375G>C	p.Gln2125His	NM_014246.1	Missense	46.0	315	0	Novel	0.12	0.614
DACT1	B04	chr14:59112534	c.1193C>T	p.Ala398Val	NM_016651.5	Missense	49.8	271	0	rs761311196	0.31	0.001
	B13	chr14:59113092	c.1751T>A	p.Leu584Gln	NM_016651.5	Missense	5.5	127	0	Novel	0.01	0.859
DVL1	B13	chr1:1273428	c.1568G>T	p.Cys523Phe	NM_004421.2	Missense	8.9	101	0	Novel	0.62	0.785
DVL2	A01	chr17:7131010	c.1195A>G	p.Met399Val	NM_004422.2	Missense	49.4	1606	0.030	rs117262744	0.07	0.012
	A13	chr17:7131010	c.1195A>G	p.Met399Val	NM_004422.2	Missense	47.3	990	0.030	rs117262744	0.07	0.012
DVL3	B13	chr3:183884743	c.1178G>A	p.Ser393Asn	NM_004423.3	Missense	9.6	115	0	Novel	0.00	0.991
FZD6	B01	chr8:104342118	c.1777C>A	p.Pro593Thr	NM_001164615.1	Missense	14.5	145	0	Novel	0.02	0.944
	A07	chr8:104343607	c.1991C>A	p.Ala664Glu	NM_001164615.1	Missense	46.5	467	0.022	rsl2549394	0.03	0.012
	A13	chr8:104330902	c.262C>G	p.Gln88Glu	NM_001164615.1	Missense	50.7	820	0	Novel	0.27	0.009
	A18	chr8:104343607	c.1991C>A	p.Ala664Glu	NM_001164615.1	Missense	54.1	451	0.022	rsl2549394	0.03	0.012
	A23	chr8:104343607	c.1991C>A	p.Ala664Glu	NM_001164615.1	Missense	55.9	331	0.022	rsl2549394	0.03	0.012
PRICKLE2	B13	chr3:64133055	c.1111C>A	p.Pro371Thr	NM_198859.3	Missense	7.1	127	0	Novel	0.81	0.911
SCRIB	A05	chr8:144890963	c.1931G>T	p.Gly644Val	NM_182706.4	Missense	48.9	394	0.001	rs201104891	0.00	0.973
VANGL1	A13	chr1: 116227955	c.1121G>A	p.Arg374His	NM_138959.2	Missense	52.8	851	0	Novel	0.00	0.004
VANGL2	B19	chr1: 160393856	c.1088T>A	p.Val363Glu	NM_020335.2	Missense	5.7	122	0.001	rs761103326	0.00	0.771
	B21	chr1: 160394994	c.1392C>G	p.Ser464Arg	NM_020335.2	Missense	5.5	165	0.000	rs760566236	0.01	0.999

Altered-allele freq. in PGM (%) refers to the ratio of the times the mutation site is detected in PGM sequencing to the total number of detection times. SIFT function prediction < 0.05 indicates that the mutation has an impact on protein function, and > 0.05 indicates the mutation does not affect protein function. Polyphen score: 0.957–1, probable damage; 0.453–0.956, possible damage; 0–0.452, benign. All types of mutation were heterozygous

Table 2

Sanger validation results

Gene	Locus	Case ID	Lesion Site	Ectoderm Epidermis	Mesoderm Heart	Mesoderm Muscle	Entoderm Thymus	Entoderm Lung	Umbilical Cord	Parents Mother	Parents Father
CELSR1	chr22:46931402	A05	c.1666C>G	c.1666C>G	c.1666C>G	c.1666C>G	c.1666C>G	c.1666C>G	NM	NM	c.1666C>G
CELSR1	chr22:46785367	A07	c.6375G>C	NM	NM	NM	NM	NM	NM	NM	–
DACT1	chr14:59112534	B04	c.1193C>T	NM	NM	NM	NM	NM	NM	–	–
DVL2	chr17:7131010	A01	c.1195A>G	c.1195A>G	NM	NM	NM	NM	NM	NM	NM
DVL2	chr17:7131010	A13	c.1195A>G	NM	NM	NM	NM	NM	NM	–	–
FZD6	chr8:104343607	A07	c.1991C>A	NM	NM	NM	NM	NM	NM	NM	–
FZD6	chr8:104343607	A18	c.1991C>A	NM	NM	NM	NM	NM	NM	–	–
FZD6	chr8:104343607	A23	c.1991C>A	NM	NM	NM	NM	NM	NM	–	–
FZD6	chr8:104330902	A13	c.262C>G	NM	NM	NM	NM	NM	NM	NM	NM
SCRIB	chr8:144890963	A05	c.1931G>T	c.1931G>T	c.1931G>T	c.1931G>T	c.1931G>T	c.1931G>T	NM	c.1931G>T	–
VANGL1	chr1:116227955	A13	c.1121G>A	NM	NM	NM	NM	NM	NM	NM	NM

NM no mutation, – missing sample